Dimmable Solid State Ballast With Integral Capacitive Occupancy Sensor

Al-Thaddeus Avestruz, *Member, IEEE*, John J. Cooley, Daniel Vickery, *Student Member, IEEE*, James Paris, and Steven B. Leeb, *Fellow, IEEE*

***Abstract*—This paper describes and demonstrates an LED lighting system with an integral capacitive sensor that can detect occupancy both lighted and in the dark, and a driver ("ballast") that is dimmable over a wide range. Sensing in the dark is accomplished by taking advantage of the logarithmic relationship between LED voltage and current. The ballast uses an inductor pre-charge technique to maintain efficiency during dimming, while maintaining relevant parameters for quality of lighting (e.g., chromaticity/color cast).**

***Index Terms*—Capacitive sensing, dimming, LED driver, occupancy sensing.**

I. Introduction: Energy-Efficient Lighting Technology

NEW illumination sources and new power electronic controls for lighting have the potential to produce energy efficiency gains of 240% in the residential sector and 150% in the commercial sector [1]. In 2007, lighting accounted for 15.6% and 23.3% of all electricity consumed in the residential and commercial sectors, respectively, in the USA [1]. Efficiency gains from lighting sources and active control can substantially reduce overall energy consumption. In particular, solid-state lighting promises improved energy efficiency and long lifetime [2].

A fluorescent lamp with an integral occupancy sensor was demonstrated in [3]–[5]. By exploiting the lamp's own stray electric field, the sensor system is able to detect changes in the electric field below the lamp, which includes people, or perhaps autonomous mobile robotics that rely on machine vision. Unlike standard proximity sensors which require building planners to design for a proximity detection system that is separate from the lighting system, this proximity sensor is essentially a drop-in replacement for a standard commercial fluorescent lamp ballast.

This paper describes:

1) the application of the lamp sensor to a solid-state (LED, i.e., light emitting diode) lighting array that detects occupancy both lighted and in the dark;
2) the design and implementation of a wide dimming range LED driver ("ballast") using an inductor precharging method.

Design considerations for the ballast include those relevant to lighting, such as power efficiency and consistent color cast, or chromaticity, across dimming levels. Although a hard-switching design using freewheeling diodes is demonstrated in this paper, it is possible to use synchronous rectifiers and soft-switching such as in [6]–[8] to improve efficiency, with a tradeoff of additional active devices and related components. The effect of dc and pulse-width modulation (PWM) dimming have been studied for both red-green-blue and phosphor-based LED light sources [9]–[11]. A PWM technique, which shorts the inductor during off-periods for the LED current, is investigated in [12]. Multiple current-level driving techniques are discussed in [13] and [14]; and [15] proposes a hybrid PWM/AM dimming strategy. Not only is the effect of dimming modulation on chromaticity a concern in lighting, but also in LCD backlighting applications [16]. Although this paper only discusses operation of the LED driver in the PWM mode, the topology easily allows for operation in similar multilevel schemes where both the peak drive current and duty cycle can be independently controlled.

A PWM technique for multiple parallel LED strings that operates with power factor correction (PFC) off the ac line is described in [17], a flyback topology also with PFC is detailed in [18], and a buck-flyback with PFC for streetlight applications in [19]. If desired, PFC can similarly be applied to the ballast described in this paper.

In addition, both the ballast and the LED array topologies must be designed to support the lamp sensor electronics by driving the lamp with an alternating current to produce an alternating electric field. An overview of the lamp sensor from [3]–[5], [20], as well as electro-quasistatic modeling approaches, is discussed in Section II. The design and implementation of the ballast for the LED lamp are discussed in Section III. Finally, experimental data from the lamp sensor built around the LED lamp are presented and compared to quasistatic models in Section IV.

II. Lamp Sensor Operation and Modeling

A. System Description

The block diagram of the lamp sensor is shown in Fig. 1. A suitable lamp and electrode arrangement is depicted in Fig. 2. A typical fluorescent or LED lamp may include an electronic

Manuscript received September 30, 2010; revised January 22, 2011 and March 29, 2011; accepted April 2, 2011. Date of publication June 30, 2011; date of current version November 1, 2011. This work was supported in part by the U.S. Department of Energy and The Grainger Foundation.

The authors are with the Laboratory for Electromagnetic and Electronic Systems, Department of Electrical Engineering and Computer Science, Massachusetts Institute of Technology, Cambridge, MA 02139 USA (e-mail: avestruz@mit.edu; jjcooley@mit.edu; drv@mit.edu; bigjim@mit.edu; sbleeb@mit.edu).

Color versions of one or more of the figures in this paper are available online at http://ieeexplore.ieee.org.

Digital Object Identifier 10.1109/TIE.2011.2161057

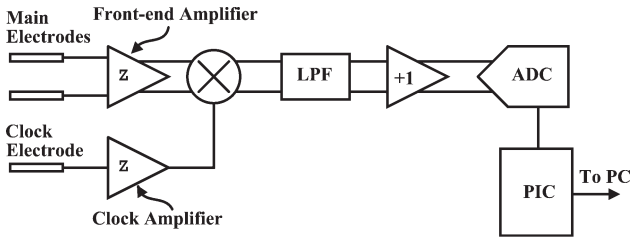

Fig. 1. Block diagram of the lamp sensor. Transimpedance amplifiers are marked with a "Z."

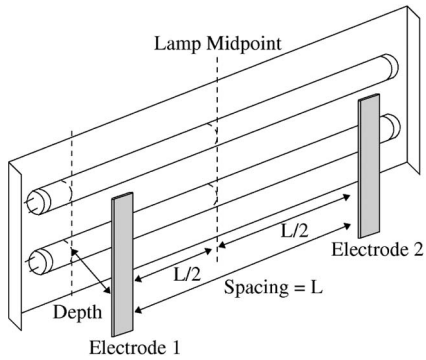

Fig. 2. Diagram of a typical two-bulb fluorescent lamp and electrode configuration. The electrodes are spaced symmetrically about the center of the lamp.

ballast that drives the bulbs with an alternating voltage at frequencies in the range of 20 to 50 kHz. As long as the lamp is driven with an alternating voltage, we have found that an electrostatic proximity sensor (lamp sensor) can be developed to measure the resulting stray electric fields below the lamp. Because a synchronous detection technique is used, the sensor is highly sensitive to the ac field from the lamp, yet insensitive to spurious fields, which is unlikely to have the correct frequency and phase. In this section, we describe the operating principles of the lamp sensor that may be applied to either a fluorescent or LED lamp. Section III describes a driver specifically suited to operating LED lamps with the proximity detector.

The lamp sensor measures low frequency (∼0.1–5 Hz) changes caused by human targets below the lamp in the high-frequency (∼50 kHz) alternating stray electric fields coupling from the lamp. The lamp sensor measures the electric fields in front of the lamp with a fully differential transimpedance front-end amplifier driven by the two electrodes depicted in Fig. 2. The front-end amplifier is fully differential because both its inputs and outputs are differential. When the electric fields measured by the two electrodes are equal, the differential measurement is balanced and the front-end output voltage is "nulled" to zero volts. Therefore, the front-end can have a very high gain without saturating its output in the absence of a detection. This very high gain is necessary to amplify the effects of small imbalances in the capacitive system below the lamp. Furthermore, the fully differential structure of the front-end amplifier relaxes the need for a specific ground reference in the lamp sensor system.

As indicated in Fig. 1, the lamp sensor uses synchronous detection to reject stray signals that differ in phase or frequency from the lamp's own excitation signal. Synchronous detection is achieved with a separate measurement of the signal source. The lamp sensor system multiplies this reference signal with the main signal using a fully differential multiplier. Whereas low-frequency occupant motion below the lamp naturally modulates the high-frequency signal measured by the front-end, the output of the multiplier (demodulator) contains the low-frequency modulations centered on zero frequency (dc). A low-pass filter (LPF) attenuates the high-frequency residue from the multiplier output to yield only the low-frequency signal. The synchronous detector and modulation-demodulation scheme also has the advantage of bypassing potentially overwhelming low-frequency 1/f noise in the front-end amplifier. Bypassing 1/f noise is critical because the signals of interest (occupancy detections) are very low in frequency. The signal of interest is amplified having been naturally upmodulated by the lamp sensor system to high-frequency (∼50 kHz). The amplified high-frequency signal is then downmodulated by the multiplier shown in Fig. 1 after amplification. Meanwhile, the low-frequency 1/f noise generated within the front-end amplifier is upmodulated by the multiplier to high frequency and attenuated by the ensuing LPF. This signal detection scheme is not unlike chopper stabilization of op-amps for elimination of low-frequency noise, detection in an AM (amplitude modulation) radio, or the so-called "lock-in" amplification technique for frequency specificity. Note that this system comprises a suppressed-carrier AM modulation-demodulation signal chain. That is, when there is no detection, there is also no carrier signal measured by the sensor. This is fundamentally why a "clock electrode" (depicted in Fig. 1) is necessary to obtain a phase and frequency reference for the desired signal.

Measurement of the electric field can be taken as a measurement of the two electrode potentials (at electrode 1 and electrode 2 in Fig. 2) referenced to some arbitrary potential. This corresponds to a voltage-mode measurement and requires a high input impedance measurement device. Alternatively, the electric field measurement can be taken as a measurement of the current shunted between the electrodes when they are connected by a short circuit. This corresponds to a current-mode measurement and requires a low input impedance measurement device. In the lamp sensor, a fully differential current-mode amplifier is used as the front-end amplifier depicted in Fig. 1. Reference [21] details the behavior and operating principles of fully differential amplifiers like the one used here. In [5], we reported 11 ft. of detection range between the lamp and the closest edge of a human target. For a detailed description of the lamp sensor operation, see references [5], [4], and [20].

B. Capacitive Modeling

The electric field measurement may be modeled as a measurement within a capacitive network. Such a capacitive network may be comprised of the capacitances connecting all of the conducting objects in the system. This abstraction is a starting point for qualitatively understanding the behavior of the lamp sensor system and its key features. Implicit in this abstraction is that the objects of interest can be represented by conducting surfaces. While some objects in the system are obviously well represented as conducting surfaces (e.g., the electrodes), the fluorescent lamp bulbs as well as the human

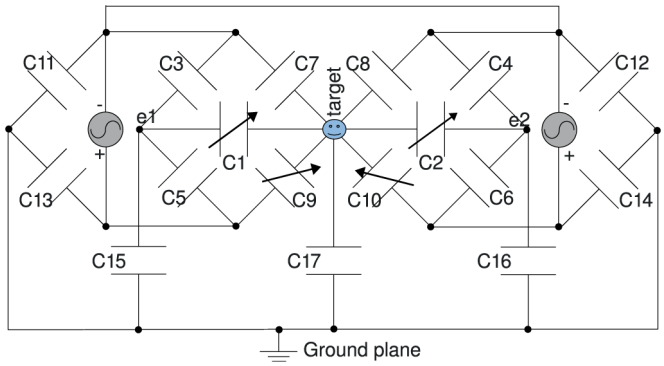

Fig. 3. Capacitive model of fluorescent lamp sensor.

target are also represented this way. References [22]–[24] describe the implications of approximating a human as a conducting shell. Reference [5] motivates the treatment of the bulb surfaces as voltage or low-impedance sources rather than current or high-impedance sources in the capacitive system. Reference [25] discusses the approximation of lumping each of the bulbs into "positive" and "negative" source ends. Furthermore, the floor below the lamp is taken as a conducting plane and could be arbitrarily chosen as the potential reference (ground) for the system.

Having these assumptions, we can build a capacitive model like the one proposed in Fig. 3 by accounting for capacitances between the conducting objects in the lamp sensor system. Accurate modeling of the lamp sensor system using this modeling approach typically requires the use of capacitance extraction software. Note that the capacitive model pictured in Fig. 3 differs from the electrostatic model described in Section IV because the low-potential source ends of the lumped signal sources are not earth grounded.

An electro-quasistatic analysis from [26] is compared to results in Section IV.

III. Power Electronic LED Drive and Dimming

Power electronic drives represent a significant efficiency improvement over linear power sources. In LEDs, light output is best controlled by regulating current. Some difficulties in using the terminal voltage as the control include a negative temperature coefficient that leads to thermal runaway and a poorly behaved exponential relation to power output.

The salient characteristic of a linear regulator is that a voltage is dropped across an element that continuously carries current, resulting in an inescapable power dissipation. Linear current regulators can use active devices in either open-loop (e.g., current mirror) or closed-loop (e.g., op-amp with a pass transistor). A voltage source with a series resistor is also used in driving LEDs—the underlying approximation is that the voltage drop across the resistor is large, hence approximating a current source, which means that it is guaranteed that power is dissipated as heat by the resistor. This approximation weakens at low current levels when dimming, resulting in a drifting current level and hence light output.

PWM of the current is an effective approach to driving an LED. Not only is there an advantage in efficiency, but a number of studies have suggested that there may be an advantage to the quality of lighting [9]–[11]. There are a number of choices for the design of a switching current source. Our design was based on several requirements, which include a bipolar source for proximity sensing, square current pulses for color quality, and a wide dimming range.

A. High Brightness LED Modules

Currently, we use commercially available modules with 14 LEDs within a diode bridge. Because these modules were originally intended to replace halogen lighting in low-voltage 60-Hz sockets, slow recovery rectifier diodes were used in the bridge, resulting in voltage waveform distortion and power loss when driven by a high-frequency inverter. The solution is to use diodes with better recovery characteristics. As we see in the driver design below, the inverter operates at frequencies just above the audio upper limit of about 20 kHz, yet below frequencies where more expensive high-performance diodes are needed.

The partitioning of these LEDs into bridged segments is an important consideration for capacitive sensing because it determines the shape of the electric field source. Ultimately, the design may consist of groups of LEDs consisting of fewer diode bridges with a voltage distribution that is optimal for sensing and would result in lower cost. The use of many uniform groups of bridged LEDs provides a proof-of-principle prototype and allows a comparison with previous results using a fluorescent lamp (linear voltage profile) field source [20].

B. Switching Current Source LED Driver

We selected a topology that consists of a buck converter with a hysteretic current controller with a switching frequency in the range of a few hundreds of kilohertz and a post-inverter in the 20–30 kHz range. A hysteretic-controlled, hard-switched converter operating in the hundreds of kilohertz range provides a fast response without having a power efficiency that is overcome by switching losses. By operating the inverter in the 20–30 kHz range, capacitive sensing is effective, without driving too much reactive current into the metal fixture.

A schematic of the power system is shown in Fig. 4. The circuit is designed to operate from a 170-V dc bus (nominal rectified line voltage) driving two parallel strings of 40-mA ac LED modules antisymmetrically, which are illustrated in Fig. 5. The dc bus can of course be derived from an ac front-end and can tolerate variable levels of ripple to provide a complete ac–ac ballast solution. By operating the buck converter in the continuous inductor current mode, nearly square pulses of current are provided by the inverter to the LEDs, which has been suggested to help maintain consistent chromaticity, or "color-cast" [9]–[11]. An advantage to this topology is that it is possible to independently control both peak and average LED current, which is useful in multilevel driving schemes, while maintaining a constant brightness. The peak current is controlled by the buck converter and the duty cycle by the full bridge.

Because the full-bridge inverter is driven by a current source with free-wheel diode, D_2, no dead-time circuitry for the switches is necessary, which simplifies the design. Placing the current-sense resistor at the bottom of the bridge enables

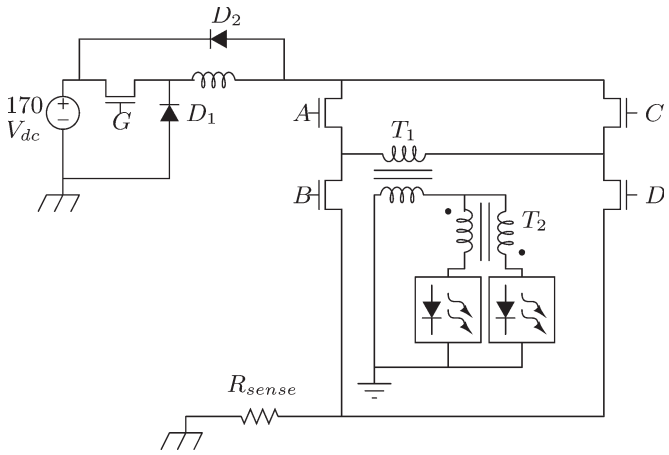

Fig. 4. Schematic of the bipolar LED driver. Transformer T_1 isolates the inverter output. Transformer T_2 matches the currents between the two LED bulbs.

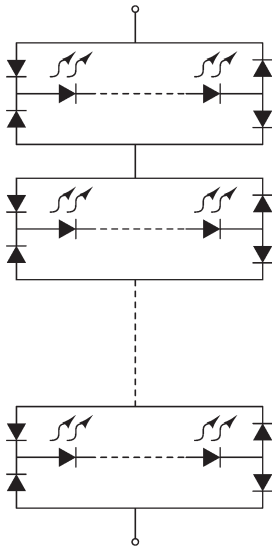

Fig. 5. Bidirectional LED modules.

ground-referenced measurement of the inductor current, which is easier than high-side differential measurements, or switch current measurements which tend to be corrupted by transients from gate drive charge injection or switch capacitance. Transformer T_1 is a 1 : 1 and provides galvanic isolation from the mains for safety and additionally allows one to choose a potential reference (e.g., fixture ground), which may result in an improved sensitivity in the lamp sensor.

An advantage to using ac to drive the LEDs is the ability to use low-cost transformers to enforce current sharing among parallel lamps at good power efficiency. Transformer T_2 is a small current balancing transformer, similar to those that are used in fluorescent lamp ballasts. The volt-second demands on this transformer are small because they correspond to the ensemble average of diode voltage mismatches among LEDs in each string.

C. Dimming and Inductor Precharging

Dimming is performed by symmetric tristate PWM at the inverter. There is a challenge in maintaining efficiency at high

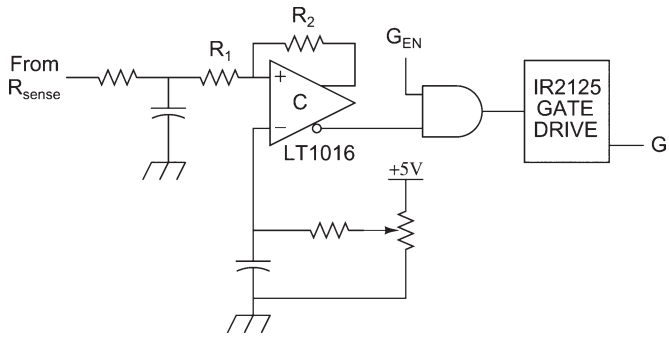

Fig. 6. Hysteretic current controller.

dimming (low-light) levels, where the duty cycle is small. Conduction losses dominate if the converter is run continuously, but alternatively, there are higher switching losses for on-off operation of the converter because square current pulses cannot be achieved without a high switching frequency. Square current pulses means a high current slew, which for on-off operation means that for a fixed input voltage, a small inductor value along with continuous inductor current is necessary, hence a high switching frequency

$$V_{input} = L\frac{dI_L}{dt} \propto L\Delta I_L f_{sw} \tag{1}$$

where ΔI_L is the inductor current ripple and f_{sw} is the switching frequency.

We developed a driving method to help overcome the challenge of efficient dimming at reasonable frequencies for hard switching, using a relatively simple converter and control scheme, which is typically a factor in lowering cost.

D. Control Circuit Implementation

The schematic for our hysteretic current-mode buck converter controller is shown in Fig. 6. A reference voltage to match the desired current (expressed as a voltage across the current-sense resistor, R_{sense}) is set with a potentiometer at the inverting input of a high-speed comparator. A positive feedback loop splits this reference into two hysteresis bands, which can be determined through superposition of the comparator output and the voltage across the current-sense resistor, V_{sense}: when the comparator's non-inverting output is LOW (0 V)

$$V_+ = V_{sense}\frac{R_2}{R_1 + R_2} \tag{2}$$

and, when the comparator's non-inverting output is $HIGH$ (5 V)

$$V_+ = V_{sense}\frac{R_2}{R_1 + R_2} + V_{out}\frac{R_1}{R_1 + R_2}. \tag{3}$$

The spread of these hysteresis bands is therefore equal to the difference between these two terms

$$\text{Hysteresis Spread} = H_+ - H_- = V_{out}\frac{R_1}{R_1 + R_2}. \tag{4}$$

Because typically $R_2 \gg R_1, V_-$ will approximately set the top hysteresis band, with the bottom hysteresis band $V_{out}R_1/(R_1 + R_2)$ below.

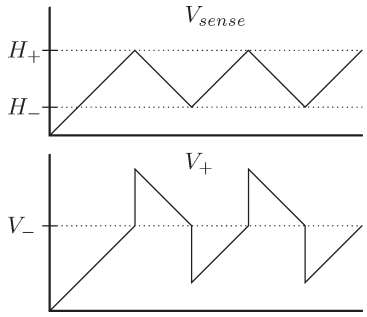

Fig. 7. Example hysteretic controller waveforms. Top: current-sense voltage V_{sense}. Bottom: Comparator non-inverting input V_+.

We set the potentiometer to obtain current regulation at 80 mA (for two LED strings at 40 mA each). We set the hysteresis spread to correspond to a 10% current ripple, with an R_{sense} of 10 Ω

$$H_+ - H_- = R_{sense}\Delta i = 10\ \Omega \cdot 8\ \text{mA} = 80\ \text{mV}. \quad (5)$$

Example control waveforms are shown in Fig. 7.

A first-order LPF is placed on the current-sense input to attenuate switching transients and prevent erroneous transitioning.

The gate enable (G_{EN}) signal is controlled by a DSPIC33FJ2560GP710 microcontroller. This signal can be used to break open the control loop and shut down the buck converter during the off-duty periods in between PWM pulses to recover inductor current.

E. Symmetric Tristate Pulse-Width Modulation

The switching pattern of the inverter generates a bipolar pulse-width modulated current through the LED strings in which the individual pulses alternate in polarity with each pulse, so there is zero dc current offset. Light output is controlled by modulating the duty of these bipolar pulses. This is known as "symmetric tristate PWM." Typical symmetric tristate PWM waveforms can be seen in Figs. 8 and 10, labeled "LED Current."

We execute symmetric tristate PWM using two modes, depending on duty ratio. These two modes are continuous current mode (performed at high duty cycles greater than 60%) and precharge mode (performed at low duty cycles below 60%). Each mode is implemented in such a way as to preserve square current pulses through the LEDs in order to improve color quality.

1) Continuous Current-Regulating Mode: In continuous current-regulating mode, the control circuit shown in Fig. 6 is run constantly ($G_{EN} = 1$ always). This means that during the off-duty period between pulses, the buck converter continues to regulate its current, which is shunted through a short consisting of two inverter switches in series: either A and B or C and D, with the corresponding complementary switches off. Keeping the buck in a continuous current-regulating state allows square LED current pulses without the need for a very large inductor di/dt. This way, we can still maintain tight current regulation using a large inductance at the buck output.

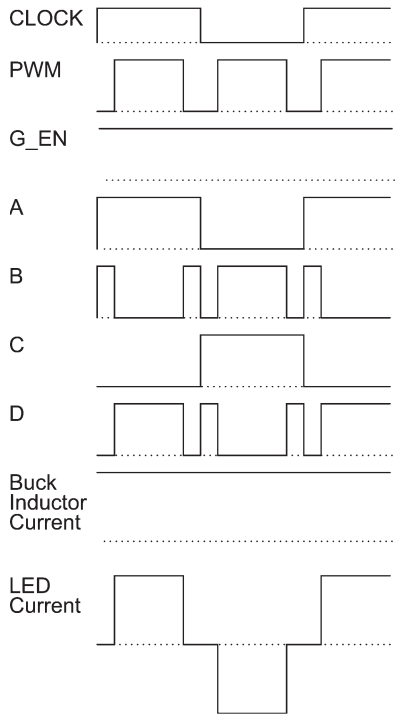

Fig. 8. Timing diagram using continuous inductor current.

Fig. 8 shows the switching pattern at high duty cycle when continuous inductor current is used. Fig. 9 illustrates the median-filtered results at 96% inverter duty cycle, where the ballast is operating in continuous current mode. *End-to-End Lamp Voltage* is the differential voltage across a single LED string. *LED Current* corresponds to the primary current of T_1 and closely represents the sum of the currents into the two parallel LED strings. A filtered version of *Clock*, with the spikes from switching transient pickup eliminated, is used for synchronization by the lamp sensor.

2) Precharge Mode: At low duty ratios, there is enough time during the off-duty periods between pulses to turn off the current controller and recover inductor current. This is done by setting the gate enable (G_{EN}) signal OFF, which opens up the current control feedback loop. All switches in the inverter are likewise turned OFF. This turns diode D_2ON, hence recovering inductor current. In order to maintain a square LED current, we precharge the inductor prior to inverter turn-on by letting the buck converter regulate into the short created by turning ON either A and B or C and D, with the complementary inverter switches OFF. Shorting the output of the buck converter in this way results in the fastest precharge for any given input voltage

$$T_{rise} = LI_{pk}/V_{in} \quad (6)$$

where T_{rise} is the rise time of the buck converter output current and L is a conservative estimate of the inductor value for all operating points and V_{in} is the input dc voltage to the buck converter, which could either be measured by the microcontroller, or set for worst case low-line voltage. Note that the inductor fall time during energy recovery is also equal to T_{rise}.

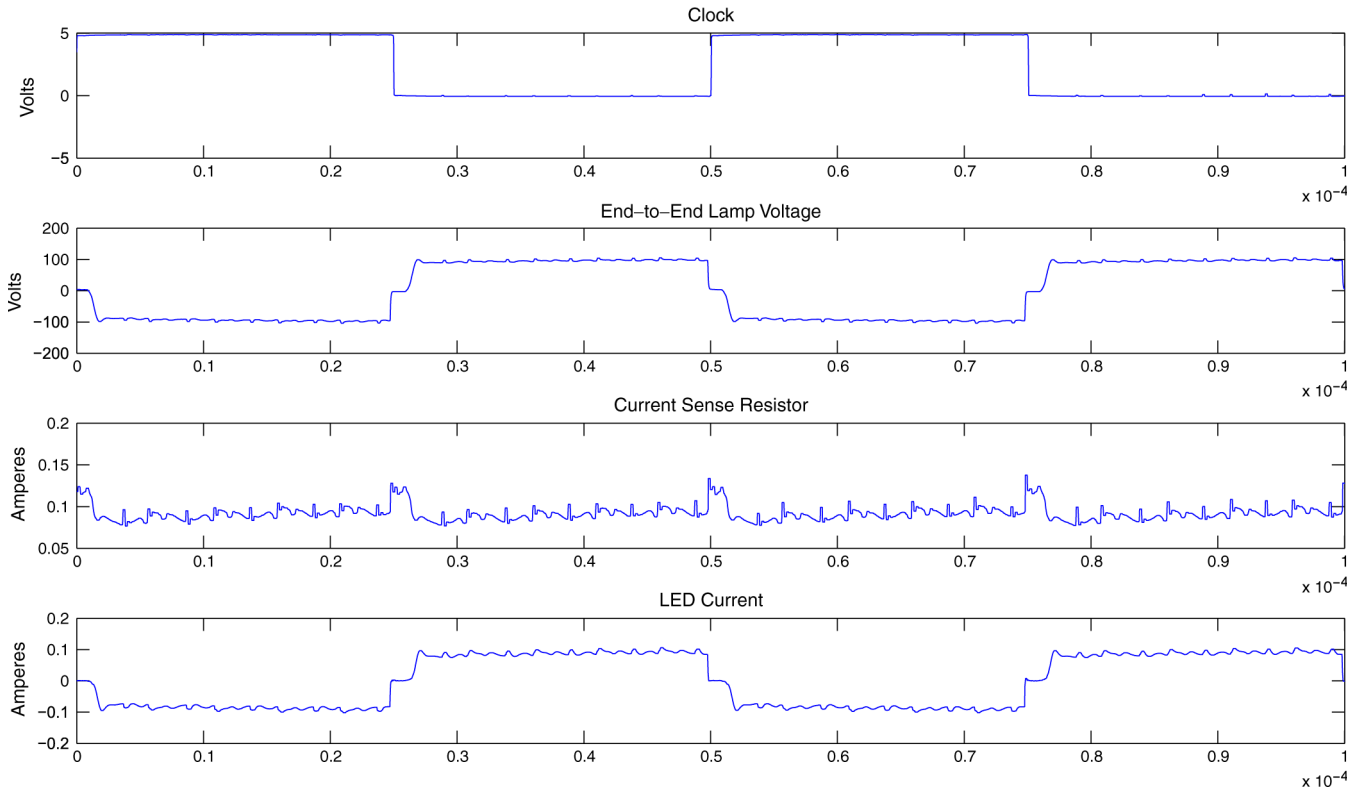

Fig. 9. Waveforms at 96% duty cycle with continuous inductor current.

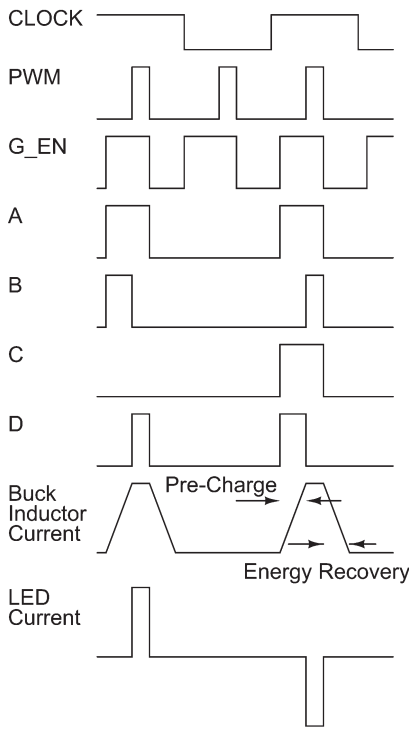

Fig. 10. Timing diagram using inductor precharging and energy recovery.

Fig. 10 shows the precharge mode switching pattern. Fig. 11 shows the median-filtered, low duty cycle waveforms where the ballast is operating in precharge mode. The *Current-Sense Resistor* waveform is the current through the resistor at the bottom of the full bridge, which represents the inductor current when the bridge switches are conducting.

By turning off the buck converter and recovering the inductor current, conduction losses are reduced for low duty ratios ($D < 60\%$). Precharging has the same advantage of allowing for a square LED current without needing a very large inductor di/dt, allowing us to utilize a large buck output inductance for tight current regulation, obviating the need for a very high switching frequency and the associated switching losses.

F. Logic Generation

The inverter switching patterns and the gate enable signal are generated by a DSPIC33FJ2560GP710 microcontroller in combination with a fast programmable logic device (PLD). The microcontroller produces three signals: CLK, PWM, and gate enable (G_{EN}). CLK controls the ballast operating frequency and corresponds to an internal clock that determines the polarity of the inverter, while PWM controls the duty ratio. G_{EN} turns the hysteretic current controller for the buck converter on and off, thereby setting the operating mode: continuous current-regulating ($G_{EN} = 1$ always) or inductor precharge. When operating in precharge mode, the duration of the G_{EN} pulse before the PWM pulse sets the precharge time.

The signals CLK, PWM, and G_{EN} are fed into the PLD, which generates the drive signals for the four inverter switches (A, B, C, D) according to a truth table, shown above as Table I. The logic states shown in Table I are listed in the sequence in which they would occur when operating in inductor precharge mode. Although, the switching patterns are created using a microcontroller and PLD for research purposes, the logic table can easily be implemented as a simple state machine in a range of low-cost, high-volume technologies.

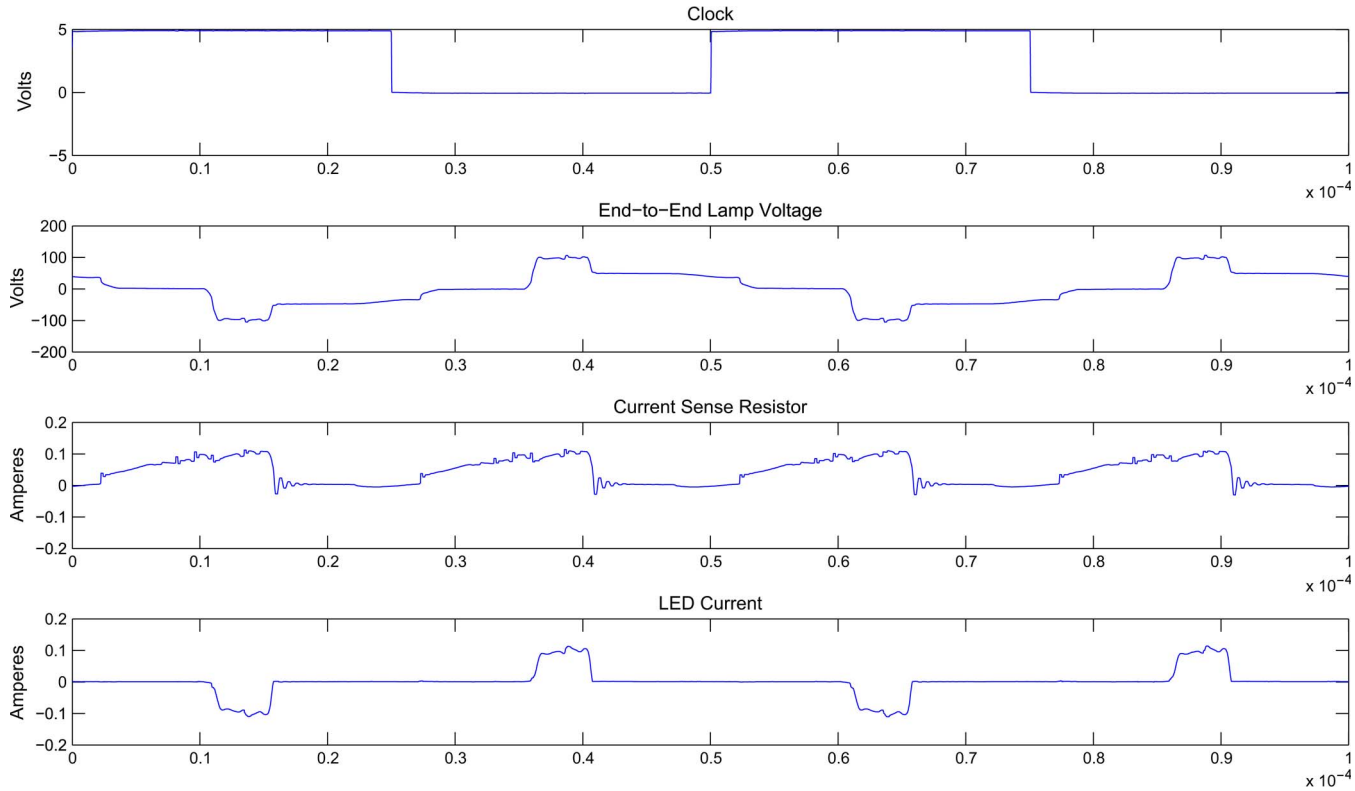

Fig. 11. Waveforms at 10% duty cycle with inductor current precharge.

TABLE I
TRUTH TABLE OF ALL POSSIBLE LOGIC STATES

MCU Signals			PLD Signals				Status
CLK	*PWM*	G_{EN}	**A**	**B**	**C**	**D**	
1	0	0	0	0	0	0	LED OFF
1	0	1	1	1	0	0	Pre-Charge
1	1	1	1	0	0	1	LED POS Current
1	0	0	0	0	0	0	LED OFF/Discharge
0	0	0	0	0	0	0	LED OFF
0	0	1	0	0	1	1	Pre-Charge
0	1	1	0	1	1	0	LED NEG Current
0	0	0	0	0	0	0	LED OFF/Discharge

G. Analysis of Power Electronic Losses

Table II illustrates power loss calculations of the hard-switched/precharging method used in this paper in comparison to maintaining the inductor current through a short similar to [12]. In addition, the decrease in power loss by using either synchronous rectifiers or soft-switching alone along with precharging is investigated. The calculations are based on IRF740 MOSFETs and MUR120 diodes. The buck inductance (L) is 10.2 mH with a dc resistance (R_{dcL}) of 10 Ω. The flat-top current (I_{peak}) to the LEDs is 80 mA with 8 mA of ripple, which results in a buck switching frequency (f_s) of 216 kHz with an inverter frequency (f_{si}) of 25 kHz. The input (V_{in}) is 170 Vdc, and the output LED voltage is 150 Vdc.

The main advantage of the precharge/energy recovery technique in comparison to only shorting the inductor is in the reduction of losses from the buck inductor at low light dimming levels. The additional losses from each precharging or energy recovery are mainly by the diode conduction during current ramp up, or down

$$P_{pc} = \frac{1}{2} V_{diode} I_{peak} T_{rise} f_{si}.$$

These additional losses are instead, when using a synchronous rectifier, dominated by the inductor during the current ramping period

$$P_{pc} = \frac{1}{3} I_{peak}^2 R_{dcL} T_{rise} f_{si}$$

which might be a slight underestimation because the dc resistance is used, but is still useful in highlighting the improvement over only shorting the inductor. In the calculation of the inductor loss during the operation of the buck converter, the dc resistance is a good approximation in the continuous current mode with small inductor ripple. Other losses associated with a synchronous rectifier include the additional gating loss, which in certain instances such as high standoff voltage and low current may dominate.

The transition switching losses for the MOSFETs were calculated using linear ramp approximations of voltage and current [27] and the gating loss using a 12 V gate drive. The main switching loss mechanism, which can be eliminated by soft-switching, is the charge stored in the output capacitance of the buck MOSFET, that is dissipated every cycle the MOSFET turns on

$$P_{cout} = \frac{1}{2} C_{out} V_{in}^2 f_s.$$

TABLE II
POWER ELECTRONIC LOSS COMPARISONS

	Shorting Inductor		**Proposed Pre-Charging**		**Synchronous Rectifier Pre-Charging**		**Soft Switching Pre-Charging**		**Units**
	95%	*10%*	*95%*	*10%*	*95%*	*10%*	*95%*	*10%*	*Dimming Duty Cycle*
Buck Converter									
Low-side Diode/MOSFET Conduction	5.4	0.6	5.4	0.6	0.4	0.04	5.4	0.6	mW
Low-side MOSFET Gating					125	13			mW
Inductor	64	64	64	6.4	64	6.4	64	6.4	mW
High-side MOSFET									
Switching Losses									
Transition	176	18	176	18	176	18			mW
Output Capacitance	190	19	190	19	190	19			mW
Gating	125	13	125	13	125	13	125	13	mW
On Resistance	3	0.4	3	0.4	3	0.4	3	0.4	mW
Current Sense Resistor	64	6.4	64	6.4	64	6.4	64	6.4	mW
Inverter									
Switching Losses									
Transition	136	136	136	136	136	136			mW
Output Capacitance	43	43	43	43	43	43			mW
Gating	14.4	14.4	14.4	14.4	14.4	14.4	14.4	14.4	mW
On Resistance	7	7	7	0.7	7	0.7	7	0.7	mW
Precharge/Energy Recovery									
Diode/MOSFET Conduction Loss				11.5		0.6		11.5	mW
Inductor				2.6		2.6		2.6	mW
Total Loss	747	250	747	192	866	192	297	70	mW
Power Delivered	11.4	1.2	11.4	1.2	11.4	1.2	11.4	1.2	W
Dc-to-Output Efficiency	93.9%	82.9%	93.9%	86.2%	92.9%	86.2%	97.2%	92.4%	

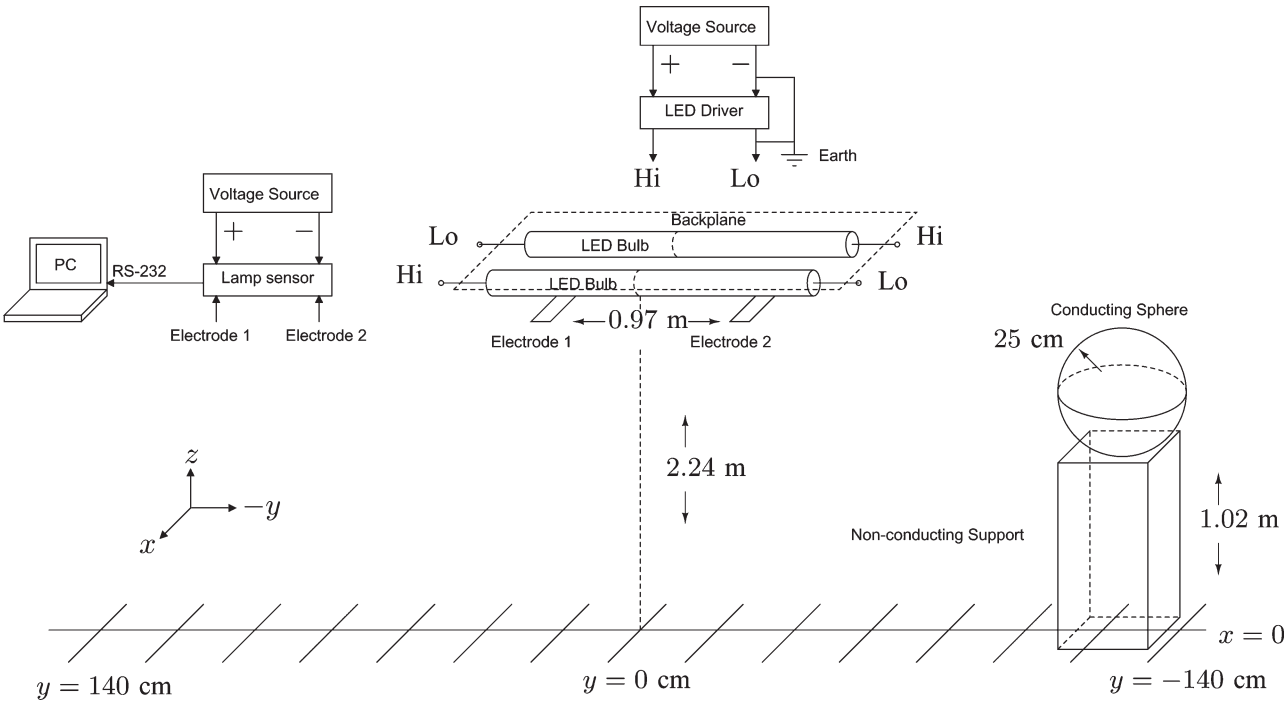

Fig. 12. Experimental setup.

Different conversion efficiencies are given only as an index for comparison because only relevant or dominating loss mechanisms are considered. Several tradeoffs can be made to improve efficiency. For example, lower current MOSFETs with higher on-resistance, but lower output capacitance and gate drive charge might be used instead of the IRF740. Also, a physically larger inductor with lower losses might be used, but this would impact power density. The purpose of the power electronic design is to provide a ballast, which supports proximity sensing, that can be modified to take into consideration the many requirements for a particular lighting use case.

IV. EXPERIMENTAL SETUP AND RESULTS

The experimental setup of the LED lamp and lamp sensor electronics is shown in Fig. 12. The lamp sensor output was measured as a conducting sphere (the target) was passed under the lamp. Data was taken with the target fixed at 20-cm intervals

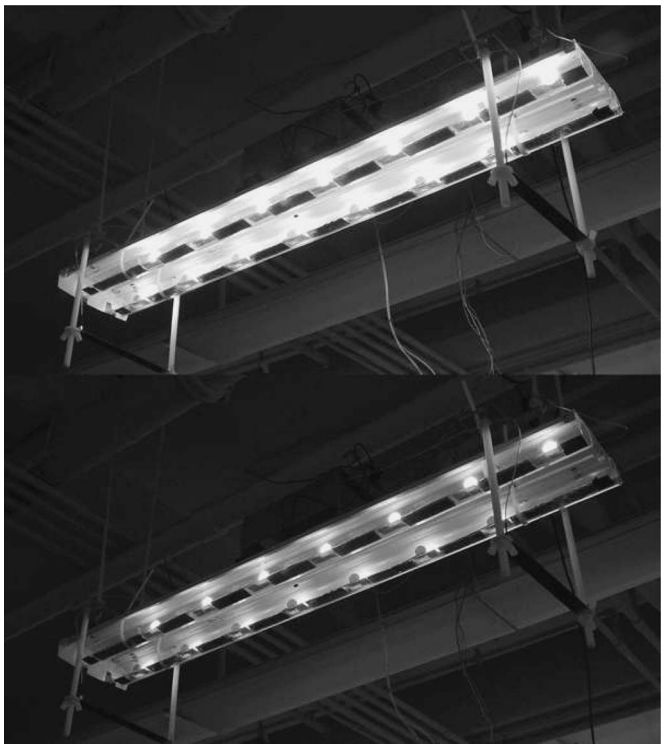

Fig. 13. Photograph of the LED lamp. Top: bright, Bottom: dim.

in the y-dimension as depicted in Fig. 12. For each interval, the lamp sensor output data was averaged for 20 s. The experiment was iterated for three lamp power settings "bright" (Duty ratio of 96%), "medium" (Duty ratio of 60%)", and "dim" (Duty ratio of 20%). A photograph of the lamp under the "bright" and "dim" settings is shown in Fig. 13. The experiment was also repeated for three x-displacements: 0 cm, 22 cm, and 45 cm.

The analytical approach described in Section II was also used to model the lamp sensor system. The electrostatic model of the lamp sensor consisted of conducting spheres representing the source nodes, electrodes, and the target. The calculated difference between the electrode potentials was taken to be proportional to the output of the lamp sensor. Also, the floor was taken to be a conductor, so the model also consisted of image spheres below the plane of the floor. Finally, the potential of the "Lo" source nodes and of the plane of the floor was assumed to be earth ground.

To compare the analytical approach to measured data, the signal source parameters used in the electrostatic model were first calibrated. A "training run" consisted of taking measured data from the lamp sensor for known x and y displacements. Then, an iterative least-squares optimization method was used to infer the effective signal source parameters based on the measured data.

In the least-squares optimization method, the signal source parameters were first guessed. Then, the results of predicting the lamp sensor output using the electrostatic modeling approach from Section II and the guessed signal source parameters were compared to the measured data. Depending on the mean squared error between the predicted and measured data, the signal source parameters were perturbed and the process was repeated. This iterative process continued until the mean

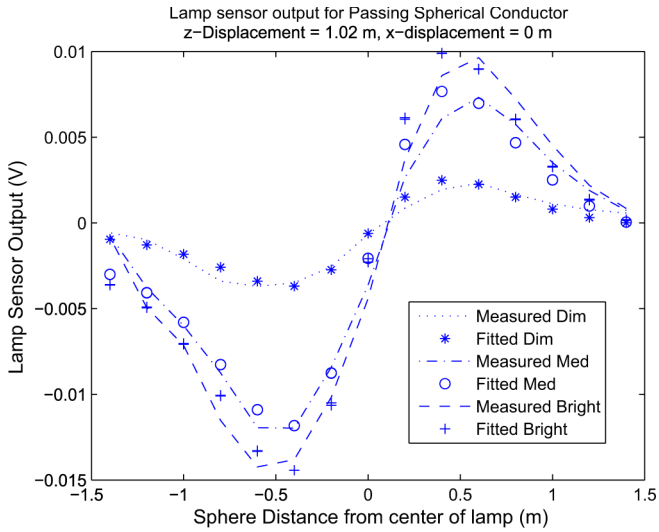

Fig. 14. Training runs (source calibration) $x = 0$ cm.

squared error between the predicted and measured lamp sensor output were below a certain threshold. The signal source parameters from the last iteration were then taken as the actual effective signal source parameters in the lamp sensor system.

The measured and fitted data in Fig. 14 correspond to training runs for each of the three lamp power settings. For each lamp power setting, we have different effective signal source parameters. Those effective signal source parameters were used to predict the lamp sensor response for different x-displacements. Fig. 15(a)–(c) compare those predictions to measured lamp sensor data at x-displacements of 22 cm and 45 cm for each of the three lamp power settings (dim, medium, and bright). The results in Fig. 15 show that the modeling approach described in Section II yields predictive power for design-oriented estimation of the lamp sensor output voltage in response to a target.

A. Dark Occupancy Sensing

In this section, we address the ability to sense occupancy in the dark, which is relevant to the use cases such as entry into a dark room. In this section, we demonstrate excellent occupancy sensing at very low LED current levels. In fact, from the brightest to essentially dark there is about a three order of magnitude difference in power level, yet the electric field source for sensing drops by only a factor that is less than a half.

In Fig. 11, a duty-cycled LED current also results in the lamp voltage pulsating. This voltage is proportional to the electric field that drives the lamp sensor. From Fig. 1, the signal that is detected is an averaged magnitude that is proportional to the duty cycle. This means that as the lamp is dimmed, the sensor voltage output decreases proportionally, which can be observed in Fig. 14. Despite the decreased voltage levels, the ouput voltage is above the detection noise floor for a wide range of dimming levels.

A special case arises in dark occupancy sensing, when one is no longer concerned about maintaining a constant peak LED current, hence relaxing the consideration for chromaticity. In this case, the LEDs can run at very low current levels at 50%

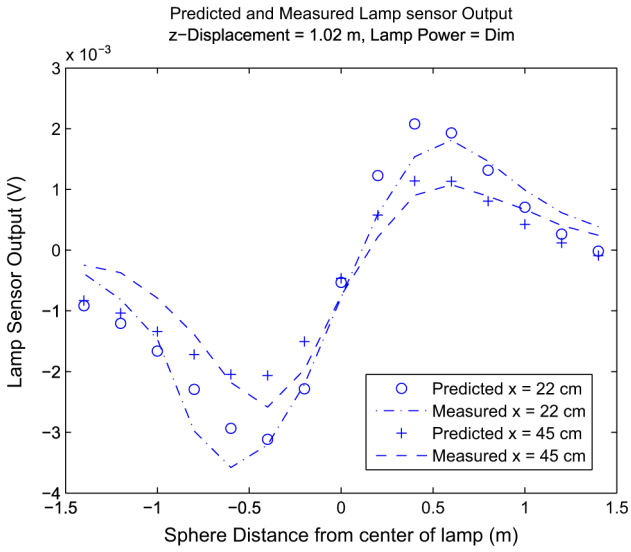

(a)

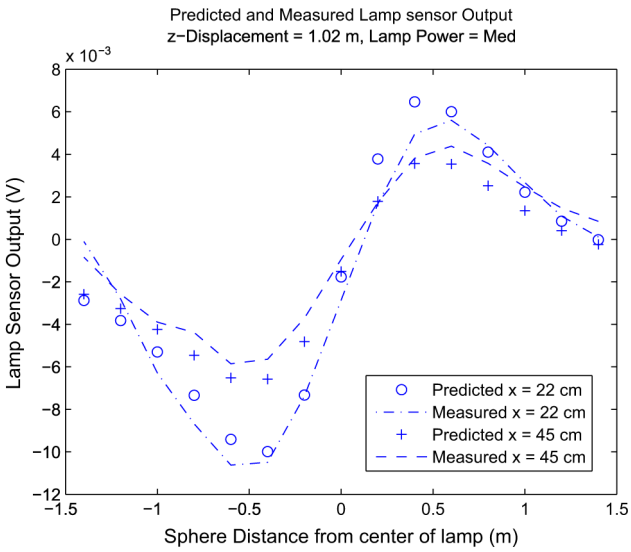

(b)

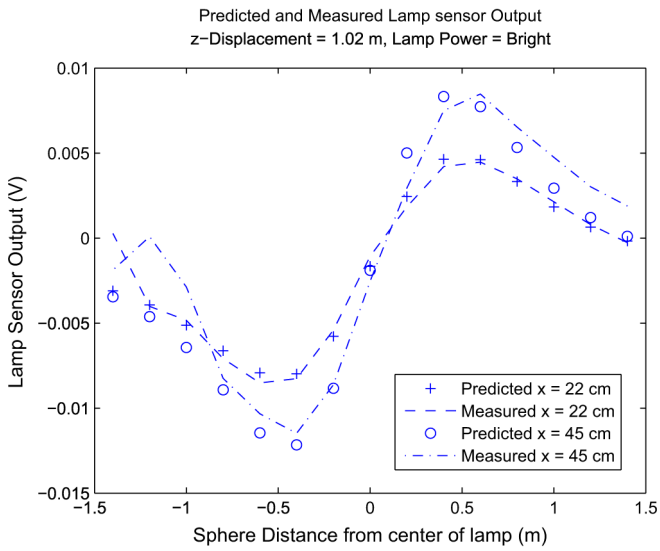

(c)

Fig. 15. LED lamp sensor measured and predicted responses. (a) Dim. (b) Medium. (c) Bright.

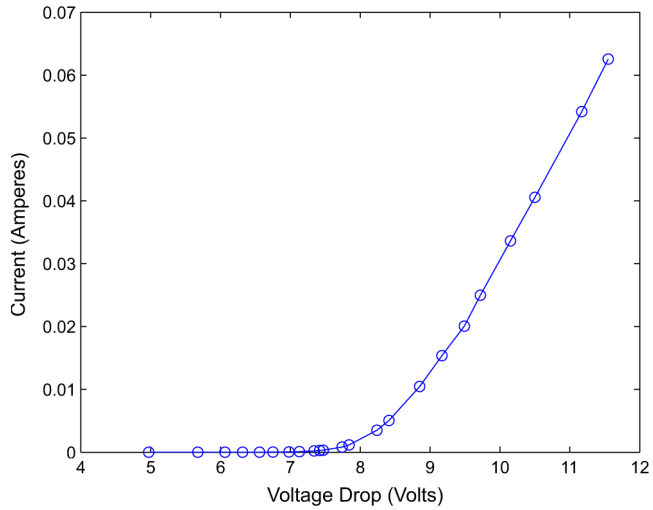

(a)

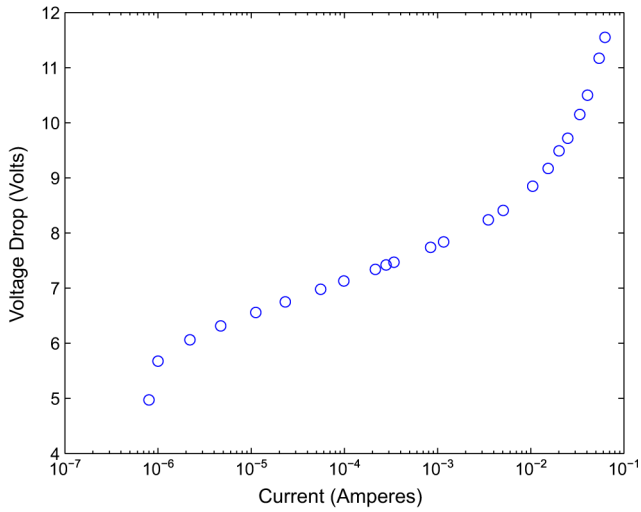

(b)

Fig. 16. I–V curve of LED lamp module. (a) is the classic diode characteristic, but closer inpection of the log plot in (b) reveals the non-idealities in real devices.

duty cycle. This is advantageous, because as we observe in Fig. 16(b), the voltage drop across one LED module changes roughly logarithmically with current. This means that most of the voltage that drives the sensing is maintained at very small current levels using the maximum available duty cycle, which results in the largest output voltage signal when using the demodulation scheme discussed in Section II.

The result for sensing in the dark is compared to sensing at moderate lighting levels in Fig. 17. A careful comparison shows that there is actually an increase in the output signal at low LED current levels. This may be attributed to a shift in the electric field distribution from the LED lamps as we vary from low to high currents. At low current levels, the shape of the electric field is dominated by parasitic capacitances from the modules to the housing, as well as the capacitances associated with LEDs at small bias. At higher current levels, the effective resistance of the LEDs decreases, which results in a different type of distribution. The dynamics and geometry of this process are complicated and are currently under investigation.

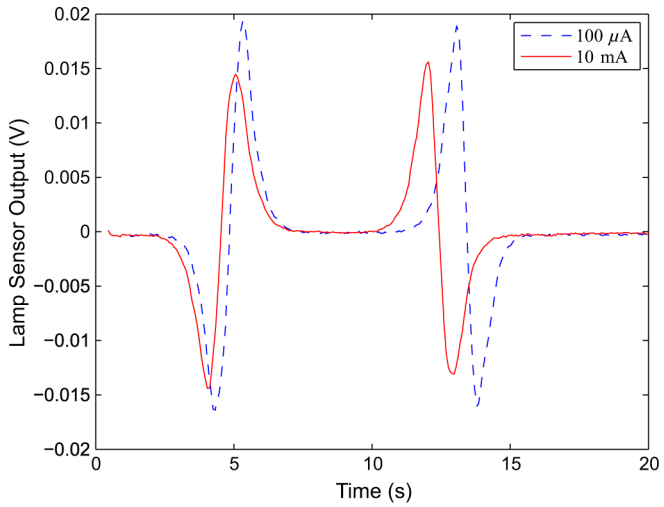

Fig. 17. Comparison of capacitive sensor output at dark (100 μA) and lighted (10 mA) LED current levels for an average height subject walking back and forth along the axis of the lamps.

V. Conclusion

Reference [28] is one of many references that discuss curtailed demand and its value in the energy market. In curtailed demand, the supply company reduces the effective energy demand by reclaiming unused or wasted energy. Reference [28] cites the sophisticated planning and knowledge of building characteristics necessary to implement curtailed demand and suggests that it can only be effective if "sensing and switching can be done cheaply" and with "a high level of automation." In particular, there is a great interest in controlling lighting to optimize energy consumption. Lighting in commercial and residential spaces consumes a significant portion of the end use demand for delivered energy in the U.S. In 2005, lighting consumed 0.73 Quadrillion Btu (QBtu) in the residential sector and 1.18 QBtu in the commercial sector [29].

This paper has presented a ballast or solid-state lamp driver that is suitable for dimmable operation of solid-state or LED lighting. The ballast design permits the possiblity for chromaticity control even at lower switching frequencies for the power electronic current drive, which results in the ability to use hard switching as opposed to resonant topologies, hence resulting in a relatively simple converter and control scheme. The ballast described in this paper also creates the correct lamp current waveforms to permit a solid-state lamp to function effectively as a proximity sensor for occupants, not just for motion as is typically deployed today. This opens the door to distributed, autonomous control for lighting. That is, light fixtures can automatically alter their illumination based on the presence or absence of occupants, and any other important environmental variables such as time of day, through the actions of an embedded controller. The proximity sensor does not require motion or other intrusive occupant behavior to function. It is sensitive directly to the dielectric presence of an occupant. Interfacing the lamp sensor with a dimming ballast creates a smart auto-dimming lamp that can use the lamp sensor's occupancy detections to appropriately dim or brighten.

This paper has also demonstrated an electro-quasistatic model that accurately predicts the behavior of the proximity sensor for both fluorescent and solid state lamps. The model can be used by building designers to predict detection range given a particular configuration of luminaire. It can also be used to select a luminaire design to achieve needed detection range.

The incorporation of automatic proximity detection in solid state lighting could be a "game changing" addition to solid-state lamps that accelerates their acceptance.

References

[1] *Annual Energy Outlook 2009*, Energy Information Administration: United States Department of Energy, Mar. 2009.

[2] D. Steigerwald, J. Bhat, D. Collins, R. Fletcher, M. Holcomb, M. Ludowise, P. Martin, and S. Rudaz, "Illumination with solid state lighting technology," *IEEE J. Sel. Topics Quantum Electron.*, vol. 8, no. 2, pp. 310–320, Mar./Apr. 2002.

[3] J. J. Cooley, A.-T. Avestruz, S. B. Leeb, and L. K. Norford, "A fluorescent lamp with integral proximity sensor for building energy management," in *Proc. IEEE PESC*, Jun. 2007, pp. 1157–1163.

[4] J. J. Cooley, A.-T. Avestruz, and S. B. Leeb, "An autonomous distributed demand-side energy management network using fluorescent lamp sensors," in *Proc. IEEE PESC*, Jun. 2008, pp. 3907–3916.

[5] J. J. Cooley, "Capacitive sensing with a fluorescent lamp," M.S. thesis, MIT, Cambridge, MA, 2007.

[6] I.-H. Oh, "A soft-switching synchronous buck converter for zero voltage switching (ZVS) in light and full load conditions," in *Proc. 23rd Annual IEEE APEC*, 2008, pp. 1460–1464.

[7] K. I. Hwu and Y. T. Yau, "Simple design of a soft-switching buck converter," in *Proc. IEEE ICSET*, 2008, pp. 410–414.

[8] J.-H. Park and B.-H. Cho, "Nonisolation soft-switching buck converter with tapped-inductor for wide-input extreme step-down applications," *IEEE Trans. Circuits Syst. I, Reg. Papers*, vol. 54, no. 8, pp. 1809–1818, Aug. 2007.

[9] M. Dyble, N. Narendran, A. Bierman, and T. Klein, "Impact of dimming white LEDs: Chromacity shifts due to different dimming methods," in *Proc. 5th Int. Conf. Solid State Light.*, vol. 5941, *Proc. SPIE*, Bellingham, WA, 2005, pp. 291–299.

[10] Y. Gu, N. Narendran, T. Dong, and H. Wu, "Spectral and luminous efficacy change of high-power leds under different dimming methods," in *Proc. 6th Int. Conf. Solid State Light.*, vol. 6337, *Proc. SPIE*, 2006, p. 63370J.

[11] S. Muthu, F. J. Schuurmans, and M. D. Pashley, "Red, green, and blue led based white light generation: Issues and control," in *Conf. Rec. IEEE 37th IAS Annu. Meeting*, 2002, vol. 1, pp. 327–333.

[12] C. M.-S. Fu and D. D.-C. Lu, "Shorting-inductor approach for dimming high power light-emitting diodes," in *Proc. Int. Conf. PEDS*, 2009, pp. 417–422.

[13] K. H. Loo, W.-K. Lun, S.-C. Tan, Y. M. Lai, and C. K. Tse, "On driving techniques for leds: Toward a generalized methodology," *IEEE Trans. Power Electron.*, vol. 24, no. 12, pp. 2967–2976, Dec. 2009.

[14] W.-K. Lun, K. H. Loo, S.-C. Tan, Y. M. Lai, and C. K. Tse, "Bilevel current driving technique for leds," *IEEE Trans. Power Electron.*, vol. 24, no. 12, pp. 2920–2932, Dec. 2009.

[15] S. Beczkowski and S. Munk-Nielsen, "Led spectral and power characteristics under hybrid PWM/AM dimming strategy," in *Proc. IEEE ECCE*, 2010, pp. 731–735.

[16] Y.-K. Lo, K.-H. Wu, K.-J. Pai, and H.-J. Chiu, "Design and implementation of RGB LED drivers for LCD backlight modules," *IEEE Trans. Ind. Electron.*, vol. 56, no. 12, pp. 4862–4871, Dec. 2009.

[17] H.-J. Chiu, Y.-K. Lo, J.-T. Chen, S.-J. Cheng, C.-Y. Lin, and S.-C. Mou, "A high-efficiency dimmable LED driver for low-power lighting applications," *IEEE Trans. Ind. Electron.*, vol. 57, no. 2, pp. 735–743, Feb. 2010.

[18] K. I. Hwu and Y. T. Yau, "Powering LED using high-efficiency sr flyback converter," *IEEE Trans. Ind. Appl.*, vol. 47, no. 1, pp. 376–386, Jan./Feb. 2011.

[19] D. Gacio, J. M. Alonso, A. J. Calleja, J. Garcia, and M. Rico-Secades, "A universal-input single-stage high-power-factor power supply for HB-LEDs based on integrated buck-flyback converter," *IEEE Trans. Ind. Electron.*, vol. 58, no. 2, pp. 589–599, Feb. 2011.

[20] J. J. Cooley, A.-T. Avestruz, and S. B. Leeb, "A retrofit capacitive sensing and occupancy detection system using fluorescent lamps," *IEEE Trans. Ind. Electron. Spec. Issue on Modern Ballast Technol.*, Sep. 2010, submitted for publication.

[21] J. J. Cooley, A.-T. Avestruz, and S. B. Leeb, A Design-Oriented Analytical Approach for Fully-Differential Closed-Loop Op-Amp Circuits, 2010.

[22] W. Buller and B. Wilson, "Measuring the capacitance of electrical wiring and humans for proximity sensing with existing electrical infrastructure," in *Proc. Int. Conf. Electro/Inf. Technol.*, 2006, pp. 93–96.
[23] P. Shahidi and A. V. Savard, "A volume conductor model of the human thorax for field calculations," in *Proc. 12th Annu. Int. Conf. IEEE Eng. Med. Biol. Soc.*, Nov. 1990, pp. 615–616.
[24] J. R. Smith, "Electric field imaging," M.S. thesis, MIT, Cambridge, MA, 1999.
[25] J. J. Cooley, "Capacitive sensing with a fluorescent lamp and applications," M.S. thesis, MIT, Cambridge, MA, 2009.
[26] J. Cooley, D. Vickery, A.-T. Avestruz, A. Englehart, J. Paris, and S. Leeb, "Solid-state lamp with integral occupancy sensor," in *Proc. APEC*, Feb. 2010, pp. 2305–2313.
[27] G. C. V. J. G. Kassakian and M. F. Schlect, *Principles of Power Electronics*. Reading, MA: Addison-Wesley, 1991.
[28] K. Taylor, J. Ward, V. Gerasimov, and G. James, "Sensor/actuator networks supporting agents for distributed energy management," in *Proc. 29th Annu. IEEE Int. Conf. Local Comput. Netw.*, Bellingham, WA, Nov. 2004, pp. 463–470.
[29] *Annual Energy Outlook 2007*, Energy Information Administration: United States Department of Energy, Feb. 2007.

Al-Thaddeus Avestruz (M'90) received the S.B. degree in physics and the S.M. and E.E. degrees in electrical engineering from the Massachusetts Institute of Technology (MIT), Cambridge, in 1994 and 2006, respectively, where he is currently working toward the Ph.D. degree in electrical engineering at the Laboratory for Electromagnetic and Electronic Systems.

He was with several companies, including Teradyne Corporation, North Reading, MA, Thornton, Inc. (presently Mettler-Toledo Thornton, Bedford, MA), and Diversified Technologies, Inc., Bedford, MA, before returning to MIT. His current research interests include circuit design, power conversion, energy, and electromagnetic systems.

Mr. Avestruz is a member of the Industrial Electronics Society.

John J. Cooley received the B.S. degree in electrical engineering and in physics, and the M.Eng. and Ph.D. degrees in electrical engineering from Massachusetts Institute of Technology, Cambridge, in 2005, 2005, 2007, and 2011, respectively.

His interests are in electronics for building energy management and multisource power systems. He is currently with FastCAP Systems Inc., Boston, MA, where he is engaged in the design of power systems for advanced energy storage technologies in automotive and grid-level applications.

Daniel Vickery (S'10) received the B.Sc. degree in electrical engineering from Massachusetts Institute of Technology (MIT), Cambridge, in June 2010.

He is currently a Graduate Research Assistant and M.Eng. candidate in the Laboratory for Electromagnetic and Electronic Systems at MIT. His interests include power, instrumentation, and RF electronics, particularly in energy management applications.

James Paris received the B.Sc. degree in electrical engineering and the M.Eng. degree from Massachusetts Institute of Technology (MIT), Cambridge, in June 2003 and January 2006, respectively. He is a Graduate Research Assistant and Ph.D. candidate in the Laboratory for Electromagnetic and Electronic Systems at MIT.

Steven B. Leeb (S'89–M'91–SM'01–F'07) received the Ph.D. degree from the Massachusetts Institute of Technology (MIT), Cambridge, in 1993.

He has served as a Commissioned Officer in the USAF reserves, and he has been a Member on the MIT faculty in the Department of Electrical Engineering and Computer Science, since 1993. He also holds a joint appointment in MIT's Department of Mechanical Engineering. He currently serves as MacVicar Fellow and Professor of Electrical Engineering and Computer Science in the Laboratory for Electromagnetic and Electronic Systems. In his capacity as a Professor at MIT, he is concerned with the design, development, and maintenance processes for all kinds of machinery with electrical actuators, sensors, or power electronic drives. He is the author or coauthor of over 100 publications and 15 U.S. patents in the fields of electromechanics and power electronics.